Modelling and Hybrid Intelligent Control of Submarine Periscope

Ali Kazemy[1] and Mohammad Farrokhi[2,*]
Department of Electrical Engineering
* Center of Excellence for Power System Automation and Operation
Iran University of Science and Technology, Tehran 16846-13114, Iran

Abstract
In this paper, first, the dynamic equations of a submarine periscope will be extracted and verified with real data. These data are acquired from an experimental setup. Then, using a neural network, a hybrid intelligent control method will be applied to control the periscope model. This control scheme is combined of a proportional controller with a feedforward neural network to adapt the controller to the nonlinearities and parameter changing of the plant. The neural network will be trained on-line without any predefined initial weights to cope with the changes in the system parameters. Simulation results will be compared with the conventional PID controller, which reveals good performance of the proposed controller.
Keywords: *Periscope - Modelling - Intelligent control - Stabilization – Kinematics.*

Introduction
Line-of-Sight (LOS) stabilization has been widely used by many researchers for varieties of applications [1]. Periscope, which is an important equipment in submarines, is an optical instrument, which is considered to be an LOS device. In periscopes, image sequences, taken by a camera, must be stabilized for better views by the operator [2]. A common periscope structure has been depicted in Figure 1. Image sequences, taken from the sea surface, are reflected by the mirror to the camera, and observed inside the submarine by the operator. The structure of a periscope is like the gyro mirror LOS stabilization [3], [4]. Major application of periscope is in submarines but tanks use them too.

Extracting dynamic equations of submarine periscopes has advantages for research, computer simulation and model-based control design. The structure of this system is like a robot manipulator. Therefore, to obtain the dynamic equations, one can use the well-known methods like the Newton-Euler or the Lagrange-Euler methods [5], [6]. In this paper, the latter method is employed.

Artificial neural networks are powerful tools for identifying and controlling nonlinear dynamic systems. In this paper, MultiLayer Perceptron (MLP) and proportional controller are used to control the mirror orientation of the periscope [7]. The training of the neural network is performed on-line. This is mainly due to the fact that in practice there are uncertainties, perturbations, or changes in the system parameters. The simulation results will be compared with the conventional PID controller.

Forward Kinematics
To obtain the homogeneous transformation matrices, the basic method is used [6]. Figure 2 shows the link coordinate frames of the periscope shown in Fig. 1. The transformation matrices of three links are defined as follows:

$$^{0}T_1 = \begin{bmatrix} c_1 & -s_1 & 0 & 0 \\ s_1 & c_1 & 0 & 0 \\ 0 & 0 & 1 & 0 \\ 0 & 0 & 0 & 1 \end{bmatrix}, \qquad ^{1}T_2 = \begin{bmatrix} c_2 & 0 & s_2 & 0 \\ 0 & 1 & 0 & 0 \\ -s_2 & 0 & c_2 & d \\ 0 & 0 & 0 & 1 \end{bmatrix}, \qquad ^{2}T_3 = \begin{bmatrix} c_3 & -s_3 & 0 & 0 \\ s_3 & c_3 & 0 & 0 \\ 0 & 0 & 1 & 0 \\ 0 & 0 & 0 & 1 \end{bmatrix}. \tag{10}$$

Dynamic Equation of the Periscope
To derive the dynamic equations, the Lagrange-Euler method is employed. Hence, the kinetic and the potential energy of the all links must be determined.

---

[1] Ph.D student of electrical engineering, control major, ali_kazemy20@yahoo.com
[2] Associate Professor of electrical engineering, control major, farrokhi@iust.ac.ir

A. The Potential and Kinetic Energy of the First Link

Since the body of periscope is fixed to the platform, the kinetic energy of the first link is just due to the energy of servomotor. Equations (2) and (3) represent the kinetic and the potential energy of the first link, respectively.

$$k_1 = \frac{1}{2}J_1\dot{\theta}_1^2 = \frac{1}{2}J_1\omega_1^2, \tag{2}$$

$$p_1 = \frac{1}{2}m_1gd, \tag{3}$$

where J_1 and ω_1 are the moment of inertia and the angular velocity of the first link, respectively, and d is the height of periscope (Fig. 1).

B. The Potential and Kinetic Energy of the Second Link

The movement of the second link is like a see-saw. Hence, for finding the kinetic and potential energy of this link, it is divided into two parts, with half mass on either side. After finding the kinetic and potential energy of each part, the kinetic energies will be added together and the potential energies will be subtracted from each other, to find the kinetic and potential energy of the whole link. The velocity of the second link is calculated at $z_2 = b/2$ with respect to the first coordinate system, where b is depicted in Fig. 2. The position and of the second coordinate axis, with respect to the zero coordinate system, is equal to

$$\begin{bmatrix} x_2 \\ y_2 \\ z_2 \end{bmatrix} = {}^0T_1\,{}^1T_2 \begin{bmatrix} 0 \\ 0 \\ \frac{b}{2} \\ 1 \end{bmatrix} = \begin{bmatrix} \frac{1}{2}bc_1s_2 \\ \frac{1}{2}bs_1s_2 \\ \frac{1}{2}bc_2 + d \end{bmatrix}. \tag{4}$$

The velocity of the upper part is equal to the velocity of the lower part

$$v_2^2 = \dot{x}_2^2 + \dot{y}_2^2 + \dot{z}_2^2 = \frac{1}{4}b^2\left(\omega_1^2 s_2^2 + \omega_2^2\right). \tag{5}$$

Therefore, the kinetic energy of the second link is equal to

$$k_2 = 2\left(\frac{1}{2}m_2v_2^2\right) + \frac{1}{2}J_2\omega_2^2. \tag{6}$$

The potential energy of the second link is equal to

$$p_2 = \frac{1}{2}m_2gz_{21} - \frac{1}{2}m_2gz_{22} = \frac{1}{2}m_2gbc_2. \tag{7}$$

C. The Potential and Kinetic Energy of the Third Link

The third link is treated like the second link. The position of the right-half part of the mirror coordinate is equal to

$$\begin{bmatrix} x_3 \\ y_3 \\ z_3 \end{bmatrix} = {}^0T_1\,{}^1T_2\,{}^2T_3 \begin{bmatrix} 0 \\ \frac{a}{2} \\ 0 \\ 1 \end{bmatrix} = \begin{bmatrix} \frac{1}{2}a(-c_1c_2s_3 - s_1c_3) \\ \frac{1}{2}a(-s_1c_2s_3 + c_1c_3) \\ \frac{1}{2}as_2s_3 + d \end{bmatrix} \tag{8}$$

Hence, the velocity of this link is equal to

$$v_3^2 = \dot{x}_3^2 + \dot{y}_3^2 + \dot{z}_3^2. \tag{9}$$

And the kinetic and potential energy of this link is

$$k_3 = 2\left(\frac{1}{2}m_3v_3^2\right) + \frac{1}{2}J_3\omega_3^2, \tag{10}$$

$$p_3 = \frac{1}{2}m_3gz_{31} - \frac{1}{2}m_3gz_{32} = \frac{1}{2}m_3gas_2s_3. \tag{11}$$

D. Lagrangian Equation

The Lagrangian equations for the periscope can be written as

$$\begin{cases} L = k_1 + k_2 + k_3 - p_1 - p_2 - p_3 \\ \dfrac{\partial}{\partial t}\left(\dfrac{\partial L}{\partial \dot{\theta}}\right) - \dfrac{\partial L}{\partial \theta} = \tau. \end{cases} \tag{12}$$

Solving (12) yields dynamic equations as

$$\tau_1 = \left(J_1 + \frac{1}{2}m_2b^2s_2^2 + \frac{1}{2}m_3a^2\left(c_2^2 - c_2^2c_3^2 + c_2 + c_3^2\right)\right)\ddot{\theta}_1 +$$

$$+ \left(\frac{1}{2}m_3a^2c_2\right)\ddot{\theta}_3 + \left(-\frac{1}{2}m_3a^2s_2s_3c_3\right)\ddot{\theta}_2$$

$$+ m_2b^2\omega_1\omega_2s_2c_2 + \frac{1}{2}m_3a^2(-2\omega_1\omega_2s_2c_2 + 2\omega_1\omega_2c_2s_2c_3^2$$

$$+ 2\omega_1\omega_3c_3s_3c_2^2 - 2\omega_2\omega_3s_2 - 2\omega_1\omega_3c_3s_3 - \omega_2^2c_2c_3s_3$$

$$- \omega_2\omega_3s_2c_3^2 + \omega_2\omega_3s_2s_3^2),$$

$$\tau_2 = \left(-\frac{1}{2}m_3a^2s_2s_3c_3\right)\ddot{\theta}_1 + \left(J_2 + \frac{1}{2}m_2b^2 + \frac{1}{2}m_3a^2\right)\ddot{\theta}_2$$

$$+ \frac{1}{2}m_3a^2(2\omega_1\omega_2c_2c_3s_3 - \omega_1\omega_3s_2c_3^2 + \omega_1\omega_3s_2s_3^2$$

$$+ 2\omega_3c_3s_3 + \omega_1^2c_2s_2 - \omega_1^2c_2s_2c_3^2 + \omega_1\omega_3s_2$$

$$+ \omega_1\omega_2c_2c_3s_3) - \frac{1}{2}m_2b^2\omega_1^2s_2c_2 - \frac{1}{2}m_2gbs_2$$

$$+ \frac{1}{2}m_3gac_2s_3,$$

$$\tau_3 = \left(\frac{1}{2}m_3 a^2 c_2\right)\ddot{\theta}_1 + \left(J_3 + \frac{1}{2}m_3 a^2\right)\ddot{\theta}_3 + \frac{1}{2}m_3 g a s_2 c_3$$
$$+ \frac{1}{2}m_3 a^2 (-\omega_1 \omega_2 s_2 - \omega_1^2 c_3 s_3 c_2^2 + \omega_1^2 c_3 s_3$$
$$+ \omega_1 \omega_2 s_2 c_3^2 - \omega_1 \omega_2 s_2 s_3^2 - \omega_2 c_3 s_3).$$
$$(13)$$

And dynamic equations of servomotors are

$$\dot{I}_a = \frac{1}{L_a}\left(-R_a I_a - k_b \dot{\theta}_M + v_a\right),$$
$$\tau_M = -J_M \ddot{\theta}_M - B_M \dot{\theta}_M + k_a I_a$$
$$(14)$$

where I_a, R_a and L_a are the armature current, resistance and inductance respectively, k_b and k_a are motor torque constant and back-emf constant, respectively, θ_M, τ_M, B_M and J_M are the motor rotational angle, output torque, damping coefficient and rotor inertia, respectively, and v_a is the input voltage to the motor. The motor and plant parameters are written in table 1 and 2, respectively.

A comparison between the data acquired from an experimental system (Fig. 3) and the proposed model, taking the dynamics of servomotor into account, has been depicted for θ_1 (the yaw axis) in Fig. 4. The modeling error has been shown in Fig. 5. As this figure shows, the error between the experimental data and the proposed model is relatively small. The input signal, applied to the model and the real plant, is shown in Fig. 6.

Controller Design
Figure 7 shows the closed-loop control block diagram for controlling the orientation of the mirror. The neurocontroller comprises of an MLP neural network (Fig. 8). Error backpropagation training algorithm has been employed.

Simulations
The main advantage of the on-line training method is its robustness against changes in system parameters. Fig. 9 shows the tracking on the θ_2 axis (the pitch axis) with the gain of P controller equal to 10, while the damping coefficient of the plant is increased by 100% at the t=3 sec. It is obvious that the controller has a rational performance but can not adapt itself against changes in the system parameters. Moreover, there might be simultaneous changes in system parameters. Hence, to achieve better tracking performance, some adaptation algorithm in the controller structure is needed. Figure 10 shows the P controller combined with the neural network to track the reference signal. The steady state tracking error is decreased by this controller and can adapt itself to the changes in the plant parameters. Note that the computation time for the neural network is less than 0.5 ms in MATLAB software, which indicates that the proposed control method can be applied in real

time. Figs. 11 and 12 show the same results for the θ_3 (the roll axis) with the P gain equal to 20.

Conclusion
In this paper, first, the dynamic equations of a submarine periscope were extracted and verified with real data. These data are acquired from an experimental setup. Then, using a neural network, a hybrid intelligent control method was applied to control the periscope model. This control skim was comprised of a proportional controller with a feedforward neural network to adapt the controller to the nonlinearities and parameter changes of the plant. The simulation results showed good performance of the proposed controller.

Table 1 - Motor Parameters

R_a (Ω)	L_a (mH)	$K_b \left(\dfrac{\text{mV}}{\text{rpm}}\right)$	$K_a \left(\dfrac{\text{mNm}}{\text{A}}\right)$	d (m)
40.2	0.8	3.2	35.1	1.1

Table 2 - Plant parameters

$m_1 (kg)$	m_2	m_3	$a(m)$	b (m)	d (m)
30	0.08	0.5	0.03	0.08	1.1

References

1- Y. M. Liang, H. R. Tyan, H. Y. M. Liao and S. W. Chen, Stabilizing image sequence taken by the camcorder mounted on a moving vehicle, pp. 90-95, In: *Proceedings of IEEE International Conference on Intelligent Transportation Systems*, Shanghai, China, 2003.

2- A. Kazemy, S. A. Hosseini and M. Farrokhi, Target-based line-of-sight stabilization in periscopes, *15th IEEE Mediterranean Conference on Control and Automation*, Athens, 2007.

3- T. H. Lee, K. K. Tan, A. Mamun, M. W. Lee and C. J. Khoh, Composite control of a Gyro mirror line of sight stabilization platform design and auto-tuning, In: *Proceedings of 3rd IEEE World Congress on Intelligent Control and Automation*, Hefei, P.R. China, 2000.

4- B. C. Siew, B. M. Chen and T. H. Lee, Design and implementation of a robust controller for a free Gyro-stabilized mirror system, In: *Proceedings of American Control Conference*, vol. 4, pp. 2231-2235, Philadelphia, USA, 1998.

5- F. L. Lewis, C. T. Abdallah and D. N. Dawson, *Control of robot manipulators*, Macmillan Publishing Company, 1993.

6- J. J. Craig, *Introduction to robotics: Mechanics and control*, Addison-Wesley Publishing Company, 1989.

7- S. Haykin, *Neural Network: A Comprehensive Foundation*, Second Edition, Prentice Hall, 1999.
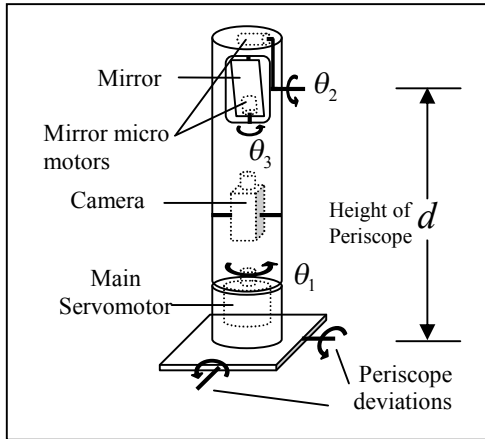
Figures

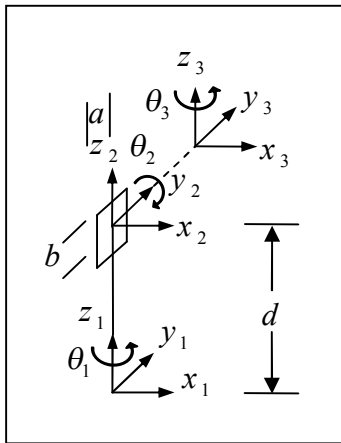
Fig. 1 Structure of a periscope

Fig. 2 Link coordinate frames of the periscope

Fig. 3 The experimental setup of periscope
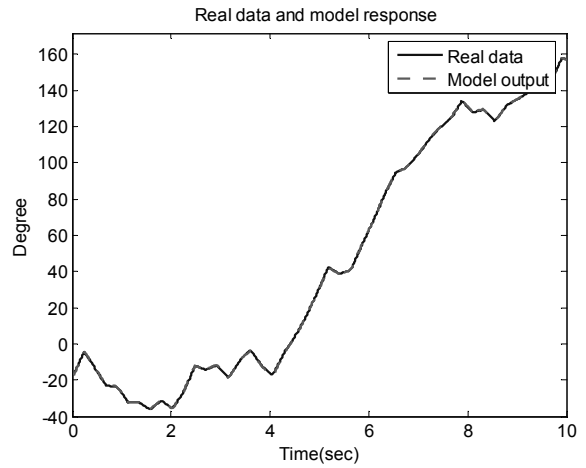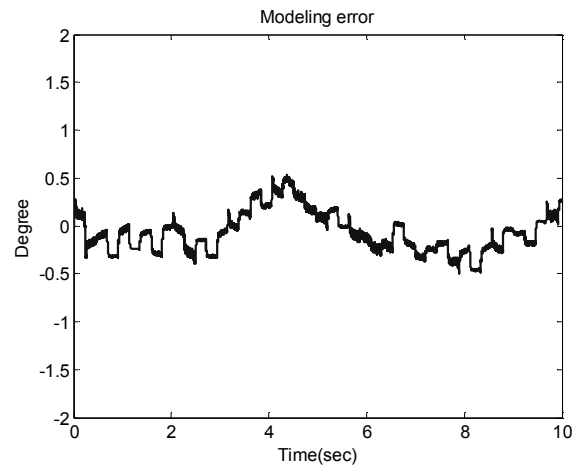

Fig. 4. Comparison of the real and model responses
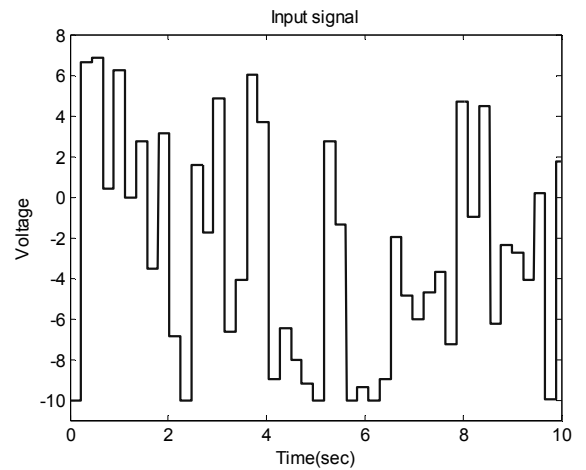

Fig. 5 Modeling error

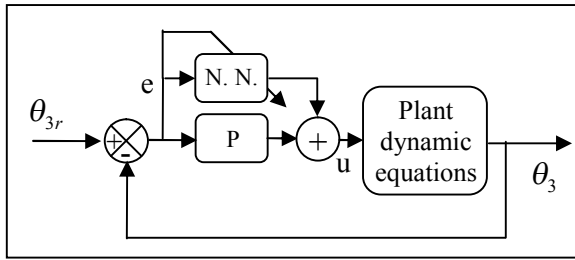**Fig. 6 Input signal applied to the servo motor in the model and in the real plant**
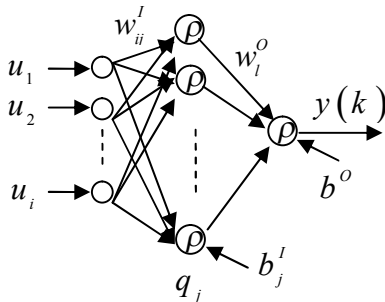
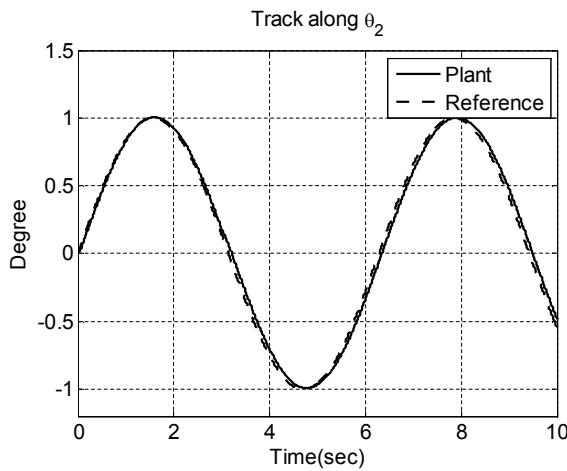**Fig. 7 Control block diagram**

Fig. 8 Structure of the neural network

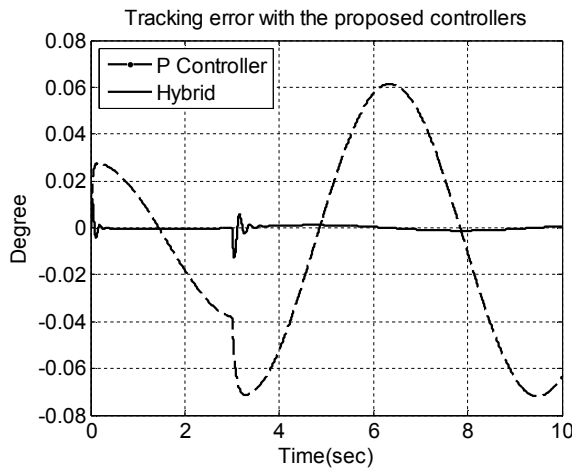**Fig. 9 Tracking along the θ_2 axis with the P controller**

Fig 10. Tracking error of the hybrid controller for the θ_2 axis
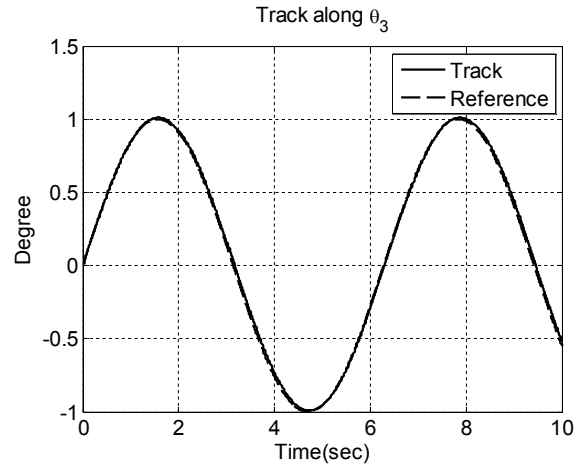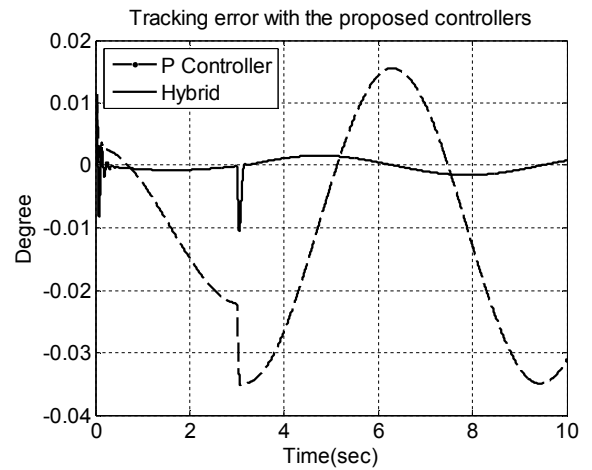

Fig. 11 Tracking along the θ_3 axis with the P controller

Fig. 12. Tracking error of the hybrid controller for the θ_3 axis